Evolution of the native oxide composition on $Al_{0.3}Ga_{0.7}As(100)$ surface under interaction with the aqueous solution of sodium sulfide

© M.V. Lebedev[1], T.V. Lvova[1], P.A. Dementev[1], I.V. Sedova[1], A.V. Koroleva[2], E.V. Zhizhin[2], S.V. Lebedev[2]

[1] Ioffe Institute,
194021 St. Petersburg, Russia
[2] St. Petersburg State University,
199034 St. Petersburg, Russia

E-mail: mleb@triat.ioffe.ru

Received September 24, 2024
Revised November 15, 2024
Accepted December 5, 2024

Morphology and composition of the oxide layers formed on $Al_{0.3}Ga_{0.7}As(100)$ surfaces under air exposure for several months, as well as their evolution under treatment with concentrated aqueous sodium sulfide solution are investigated by atomic-force microscopy and X-ray photoelectron spectroscopy. It is shown that the native oxide layer formed at the $Al_{0.3}Ga_{0.7}As(100)$ surface is non-uniform. In particular, its upper part contains III-group metal oxides and arsenic oxides, whereas the semiconductor/oxide interface is enriched with elemental arsenic. Treatment with concentrated aqueous sodium sulfide solution causes almost complete removal of oxides. After treatment the elemental arsenic coat of about ~ 1 nm thick remains, which roughness increases with the time of surface treatment.

Keywords: atomic-force microscopy (AFM), X-ray photoelectron spectroscopy (XPS), chemical etching, surface passivation, surface roughness.

DOI: 10.61011/SC.2024.11.59959.7104

1. Introduction

AlGaAs alloys are actively used in modern nanoheterostructured devices [1–8]. The technology of their formation often combines various epitaxial growth and post-growth processes. In addition, AlGaAs-based shells are widely used for passivation of nanowire surfaces [9,10]. Chemically active surfaces of III–V semiconductors, especially those containing aluminum, are covered with a disordered native oxide layer after just a short-term contact with air, which degrades semiconductor device characteristics. Therefore, the development of methods for removing the native oxide from the surface, while leaving it atomically smooth, is one of the priorities of semiconductor technology.

Treatment of the surface with various acidic solutions in an inert air-free environment enables removal of the native oxide layer from the surfaces of binary III–V semiconductors. However, aluminum oxide, which is part of the native oxide layer on the surface of aluminum-containing alloys, is difficult to remove even with the help of multi-component chemical etchants used in semiconductor technology [11,12]. It has also been found that various methods of so-called „dry" etching in gaseous media cause stoichiometry disruption in the near-surface region of alloys [13,14].

One of the efficient ways to remove the native oxide layer from the surfaces of III–V semiconductors is treatment with sodium sulfide solutions (Na_2S). It was previously demonstrated that pre-epitaxial surface preparation of various substrates in an aqueous sodium sulfide solution can significantly improve the quality of the formed epitaxial layer/substrate [15–18] interfaces. It should also be noted that the interaction between sulfide solutions and the surface of most binary III–V semiconductors is studied in detail, while the investigations of the interaction of aluminum-containing solid solutions (such as AlGaAs) with sulfide solutions are rather few [15,19], and the mechanism of such interaction is still far from being understood.

Recently it has been shown that treatment of the AlGaAs(100) surface with a concentrated aqueous sodium sulfide solution (Na_2S) leads to almost complete removal of gallium, aluminum and arsenic oxides, so that the surface remains covered by a layer of elemental arsenic with phenocrysts of residual gallium and aluminum oxides [20]. This work is concerned with the study of the morphology of native oxide layer formed on the $Al_xGa_{1-x}As(100)$ surface ($x \sim 0.3$) under air exposure, as well as its change as a result of treatment with concentrated aqueous sodium sulfide solution.

2. Experiment procedure

Layers of $Al_{0.3}Ga_{0.7}As$:Si and $Al_{0.3}Ga_{0.7}As$:Be (100), respectively of *n*- and *p*-type conductivity, a $1\,\mu$m thick and an $(1-3)\cdot 10^{17}\,cm^{-3}$ doping level were grown on *n*-GaAs(100) substrates by molecular beam epitaxy. After growth, the samples were incubated in air for 10 (*n*-AlGaAs) and 6 months (*p*-AlGaAs) to form a stable oxide layer on the surface [20].

The native oxide-covered $Al_{0.3}Ga_{0.7}As(100)$ layers were treated with concentrated (4.7 M) aqueous Na_2S solution for various times (1−12 min) and then analyzed by atomic-force microscopy (AFM) and X-ray photoelectron spectroscopy (XPS).

The surface morphology of the samples was analyzed by AFM under atmospheric conditions on a domestic device NTegra Aura (NT-MDT, Moscow) operating in semi-contact mode using NSG11 probes with a stiffness coefficient of 5 N/m and a radius of curvature of the probe needle tip of 10 nm. The scanning fields were chosen to be $3 \times 3\,\mu$m, and measurements were made in three different areas of each sample. The root mean square deviation (RMS — root mean square) was chosen as a quantitative measure of roughness. Statistical processing of AFM topography was performed using Nova software (NT-MDT). The RMS value for each sample was determined by averaging.

XPS studies were carried out using an Escalab 250Xi photoelectron spectrometer and an AlK_α source with a photon energy of 1486.6 eV. The binding energy scale was calibrated by measuring the spectra of the Au $4f_{7/2}$ (84.0 eV) and Cu $2p_{3/2}$ (932.7 eV) core levels of a special calibration sample. The vacuum level in the measuring chamber was at least $1 \cdot 10^{-9}$ mbar.

3. Results and discussion

The morphology of the *n*- and *p*-$Al_{0.3}Ga_{0.7}As(100)$ surfaces covered with native oxide layer is shown in Figure 1. It can be seen that, despite relatively long air exposure, the surfaces remain quite smooth, so that the RMS surface roughness value is 1−1.5 monolayer.

To study the components distribution over the samples depth from the surface, the spectra of different core levels with different binding energies and, thus, with different information depths defined as 3λ, where λ is the inelastic mean-free path for the corresponding photoelectrons [21], were analyzed. In particular, the core levels of gallium Ga $3d$ ($3\lambda \approx 9.1$ nm) and Ga $2p_{3/2}$ ($3\lambda \approx 3.3$ nm), arsenic As $3d$ ($3\lambda \approx 9.1$ nm) and As $2p_{3/2}$ ($3\lambda \approx 2.0$ nm) and aluminum Al $2p$ ($3\lambda \approx 8.9$ nm) were analyzed. The λ values for $Al_{0.3}Ga_{0.7}As$ were calculated using the database [22]. It should be noted that there is no aluminum core level with high binding energy suitable for analysis of chemical bonds in the near-surface region of the semiconductor.

Typical spectra of the Al $2p$, Ga $3d$ and As $3d$ core levels for *n*- and *p*-$Al_{0.3}Ga_{0.7}As(100)$ surfaces covered by a native oxide layer have been presented in [20]. Figure 2 shows the comparison of the spectra of the As $3d$ and As $2p_{3/2}$, as well as Ga $3d$ and Ga $2p_{3/2}$ core levels for the native-oxide-covered *n*-$Al_{0.3}Ga_{0.7}As(100)$ surface. The arsenic core level spectra can be decomposed into four components: the bulk As−Ga/Al, the elemental arsenic component As^0, and the two oxide components As_2O_3 and As_2O_5. The increased width of the oxide component As_2O_3 (compared to the width of the bulk component) in the spectrum of the As $2p_{3/2}$ level indicates the presence of oxides with other oxidation degrees (e.g., AsO and As_2O [23]). The large width of the As^0 component in the spectrum of the As $2p_{3/2}$ level is apparently due to the presence of several nonequivalent positions of elemental arsenic on the surface having different charge states, e.g., in „hollows“ and on „hills“.

The thicknesses (in monolayers) of the various native oxide layer components on the *n*- and *p*-$Al_{0.3}Ga_{0.7}As(100)$ surfaces calculated using formula (1). The Ga−O component in the Ga $2p_{3/2}$ spectra represents the sum of the Ga_2O and Ga_2O_3 components

Component	*n*-$Al_{0.3}Ga_{0.7}As(100)$		*p*-$Al_{0.3}Ga_{0.7}As(100)$	
	$3d$ [20]	$2p_{3/2}$	$3d$ [20]	$2p_{3/2}$
As^0	3.6	0.9	4.3	1.1
As_2O_3	2.9	3.1	2.6	2.5
As_2O_5	0.3	0.3	–	0.05
Ga−O	4.9	4.9	5.3	5.1

The surface-sensitive Ga $2p_{3/2}$ core-level spectrum can be decomposed into three components. In addition to the bulk component Ga−As the spectrum has the components shifted relative to the bulk component by 0.75 and 1.3 eV, which can be identified, respectively, with the oxides Ga_2O and Ga_2O_3 [23]. It should be noted that these oxides do not display bulk compounds of the appropriate stoichiometry, but rather surface/interface chemical bonds whose atoms may have the appropriate charge state. In the bulk-sensitive Ga $3d$ core level spectrum, these two components are difficult to distinguish and thus they are represented by a single Ga−O component with chemical shift of ~ 1 eV (Figure 2).

The layer thicknesses of each of the surface components were estimated by the formula [21]

$$d = \lambda \ln\big((I_s/I_b) + 1\big), \qquad (1)$$

where I_s is the intensity of the surface component in a core level spectrum, and I_b is the intensity of the bulk component in the corresponding core level spectrum. The layer thicknesses for gallium and arsenic oxides, as well as elemental arsenic on the *n*- and *p*-$Al_{0.3}Ga_{0.7}As(100)$ surfaces, calculated by formula (1), determined on the basis of decompositions of the bulk-sensitive and surface-sensitive spectra of the As $3d$, Ga $3d$, As $2p_{3/2}$, and Ga $2p_{3/2}$ core levels, respectively, are listed in the table. It should be noted that the layer thicknesses for the surface components obtained from Ga $3d$ and As $3d$ spectra were presented earlier in [20]. The thicknesses of aluminum oxide layers on the *n*- and *p*-$Al_{0.3}Ga_{0.7}As(100)$ surfaces obtained from decompositions of the Al $2p$ spectra were 6.6 and 7.5 monolayers, respectively [20].

It can be seen that the amounts of gallium and arsenic oxides obtained from the analysis of surface-sensitive and bulk-sensitive spectra are almost the same, while the amount

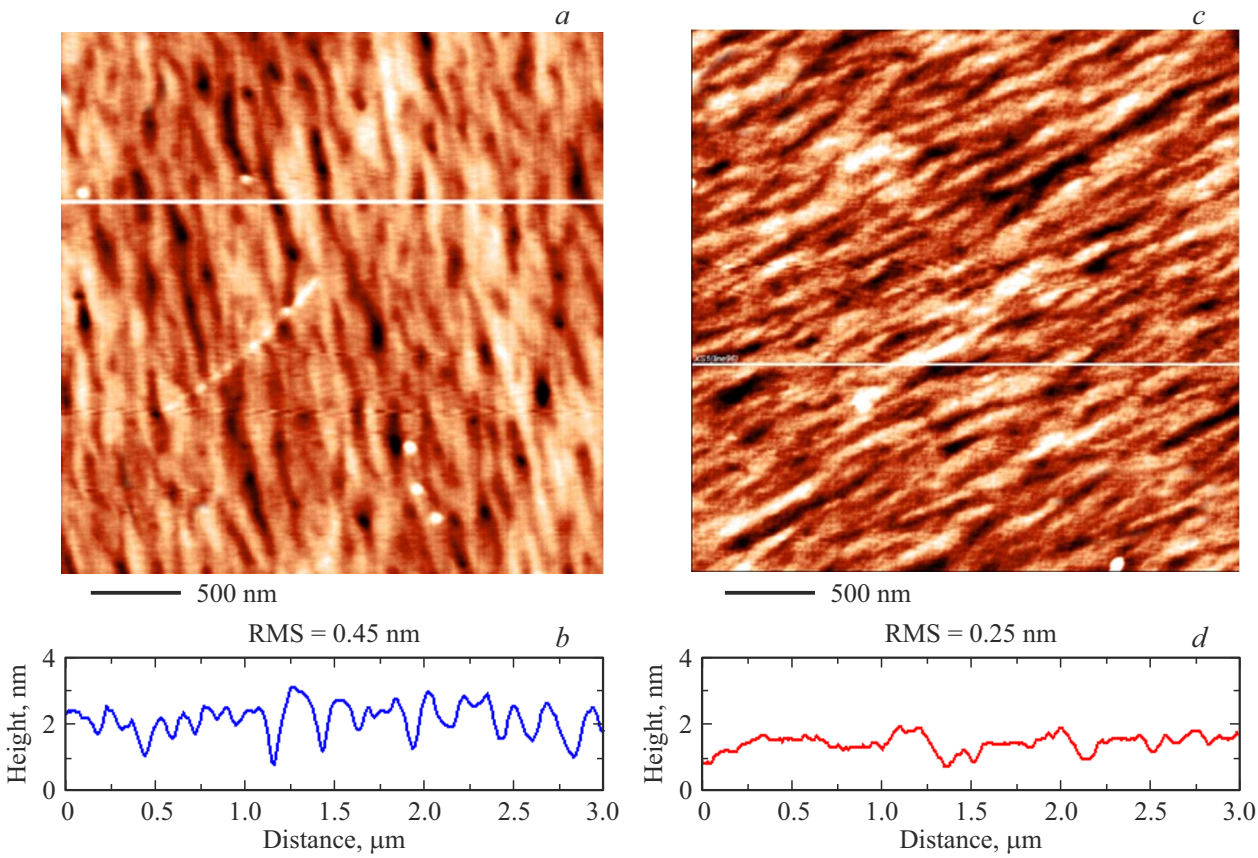

Figure 1. AFM images (*a*, *c*) and the corresponding surface profiles along the white lines (*b*, *d*) for the native-oxide covered *n*-$Al_{0.3}Ga_{0.7}As(100)$ (*a*, *b*) and *p*-$Al_{0.3}Ga_{0.7}As(100)$ (*c*, *d*) surfaces.

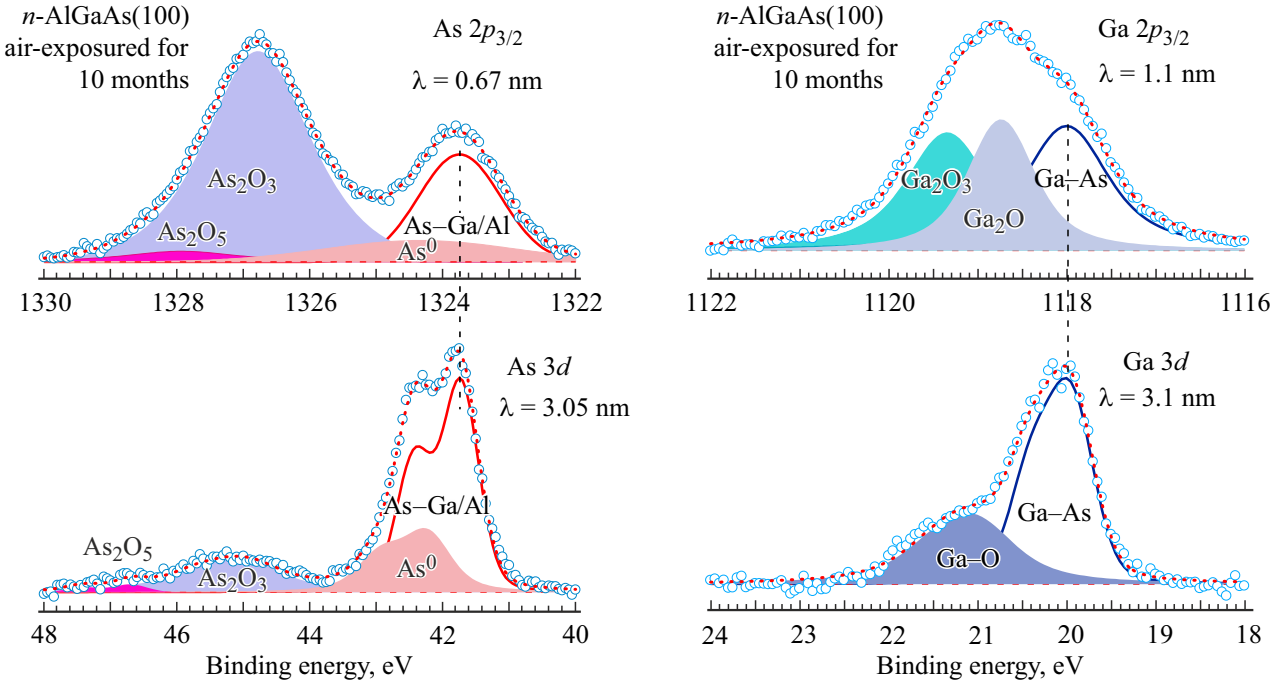

Figure 2. Spectra of As 3*d* ($3\lambda \sim 9.1$ nm) and As $2p_{3/2}$ ($3\lambda \sim 2.0$ nm), as well as Ga 3*d* ($3\lambda \sim 9.1$ nm) and Ga $2p_{3/2}$ ($3\lambda \sim 3.3$ nm) core levels for *n*-$Al_{0.3}Ga_{0.7}As(100)$ surface exposed to air for 10 months. (A color version of the figure is provided in the online version of the paper).

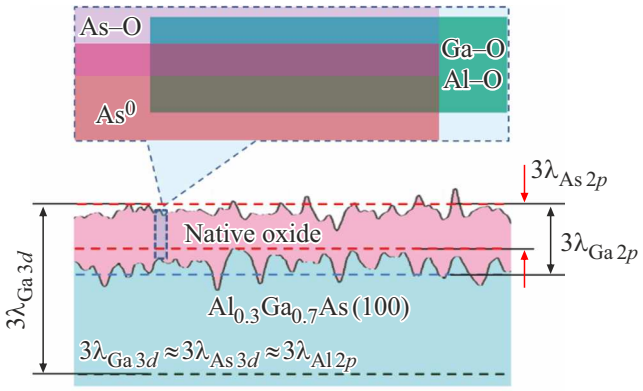

Figure 3. Schematic representation of the near-surface region of AlGaAs(100) and the structure of the native oxide layer.

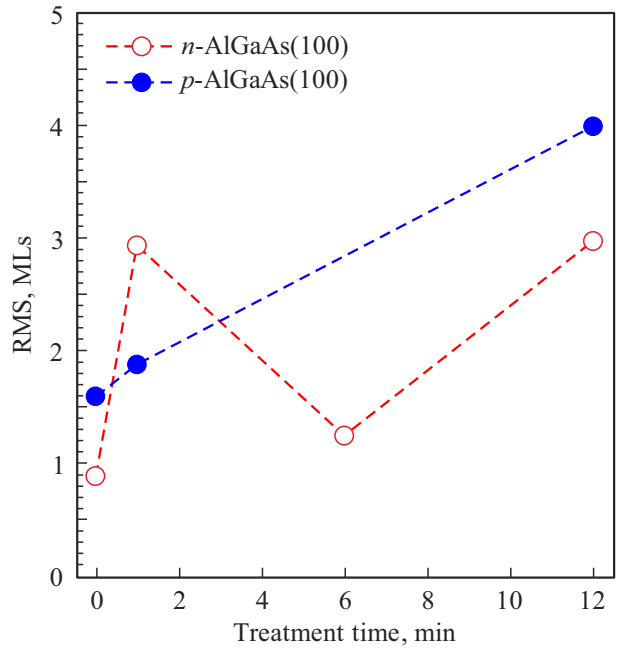

Figure 4. Variation of the RMS surface roughness of *n*- and *p*-$Al_{0.3}Ga_{0.7}As(100)$ when treated with 4.7 M Na_2S aqueous solution.

of elemental arsenic in the decomposition of the surface-sensitive spectra of As $2p_{3/2}$ in ~ 3.8 times less than that in the decomposition of the bulk-sensitive spectra of As $3d$ (see Table).

This result can be explained by assuming the roughness of the interface between the semiconductor and the native oxide layer (Figure 3). From the analysis of the thicknesses of the surface component layers, it is evident that the thickness of the native oxide layer on the considered AlGaAs(100) surfaces should not exceed 2 nm. This value approximately corresponds to the depth of the analyzed region for the photoelectrons of the As $2p_{3/2}$ ($3\lambda_{As2p}$) core level. On the other hand, the oxidation of the surface does not occur layer by layer, resulting in a rough semiconductor/oxide interface, so that some areas of the oxide layer are located deeper than the $3\lambda_{As2p}$ value (Figure 3). As has been shown [20,24,25], the boundary of the oxide layer with (Al)GaAs consists mainly of elemental arsenic (Figure 3) due to the movement of gallium and aluminum atoms towards the surface to compensate for mechanical stresses arising from the introduction of oxygen atoms into the semiconductor lattice during oxidation [25,26]. Therefore, it can be assumed that part of elemental arsenic is located in the surface inhomogeneities at a depth below $3\lambda_{As2p}$ and, accordingly, is not represented in the As $2p_{3/2}$ core level spectrum, but is clearly visible in the As $3d$ core level spectra. On the other hand, the information depth for the Ga $2p_{3/2}$ photoelectrons ($3\lambda_{Ga2p}$) is noticeably larger than $3\lambda_{As2p}$ (Figure 3), and, accordingly, the thicknesses of the gallium oxide layers estimated from decompositions of the spectra of surface-sensitive and bulk-sensitive Ga $2p_{3/2}$ and Ga $3d$ core levels are almost the same (see Table).

Treatment of the native-oxide-covered *n*- and *p*-$Al_{0.3}Ga_{0.7}As(100)$ surfaces with 4.7 M aqueous sodium sulfide solution resulted in a slight increase in the RMS surface roughness (Figure 4). At the same time, the roughness of the *n*-$Al_{0.3}Ga_{0.7}As(100)$ surface increased monotonically with processing time, while the temporal variation of the surface roughness of *p*-$Al_{0.3}Ga_{0.7}As(100)$ was more complex (Figure 4).

Figure 5 shows the spectra of As $3d$ and As $2p_{3/2}$, as well as Ga $3d$ and Ga $2p_{3/2}$ core levels for the *n*-$Al_{0.3}Ga_{0.7}As(100)$ surface treated with 4.7 M Na_2S aqueous solution for 1 min. It can be seen that after treatment with 4.7 M Na_2S aqueous solution, arsenic oxides disappear almost completely, and the content of gallium oxides (as well as aluminum oxides [20]) decreases significantly. The thicknesses of the oxide components remaining on the surfaces of *n*- and *p*-$Al_{0.3}Ga_{0.7}As(100)$ after treatment with 4.7 M aqueous sodium sulfide solution, calculated by the formula (1), are shown in Figure 6. The values calculated on the basis of decompositions of the bulk-sensitive As $3d$, Ga $3d$ and Al $2p$ core level spectra [20], and the values calculated based on decompositions of the surface-sensitive As $2p_{3/2}$ and Ga $2p_{3/2}$ core level spectra are given.

As in the case of the native oxide layer (see Table), after treatment of the surface with 4.7 M aqueous Na_2S solution, the thickness of the elemental arsenic layer obtained from the decomposition of the spectra of the surface-sensitive As $2p_{3/2}$ core level is significantly less than the thickness of the elemental arsenic layer estimated from the decomposition of the spectra of the bulk-sensitive As $3d$ core level, which indicates that part of the elemental arsenic is still located in the inhomogeneities of the semiconductor/oxide boundary below the depth of $3\lambda_{As2p}$ (Figure 3). At the same time, the thickness of the gallium oxide layer obtained from the decomposition of the spectra of the surface-sensitive Ga $2p_{3/2}$ core level appears to be significantly less than the thickness of the gallium oxide layer estimated from the decomposition of the spectra of the bulk-sensitive Ga $3d$ core level (Figure 6). This fact can be associated with the

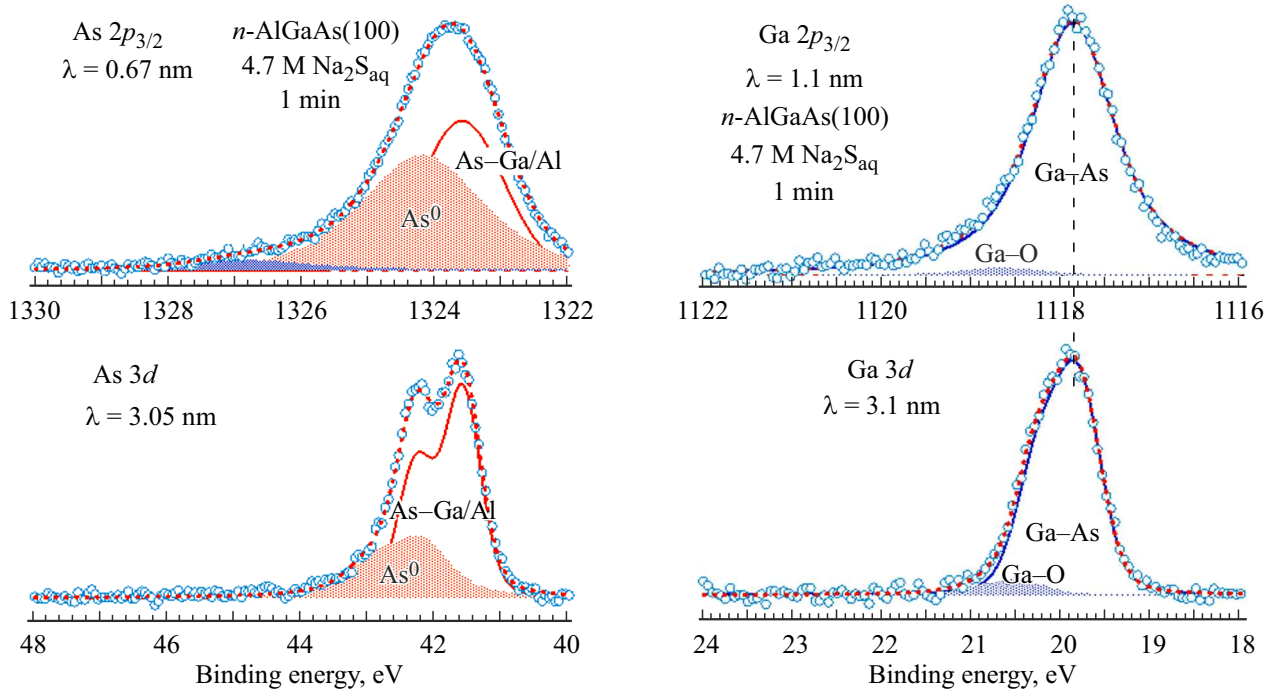

Figure 5. Spectra of As3*d* ($3\lambda \sim 9.1$ nm) and As $2p_{3/2}$ ($3\lambda \sim 2.0$ nm), as well as Ga 3*d* ($3\lambda \sim 9.1$ nm) and Ga $2p_{3/2}$ ($3\lambda \sim 3.3$ nm) core levels for the *n*-$Al_{0.3}Ga_{0.7}As(100)$ surface measured after treatment with 4.7 M Na_2S aqueous solution.

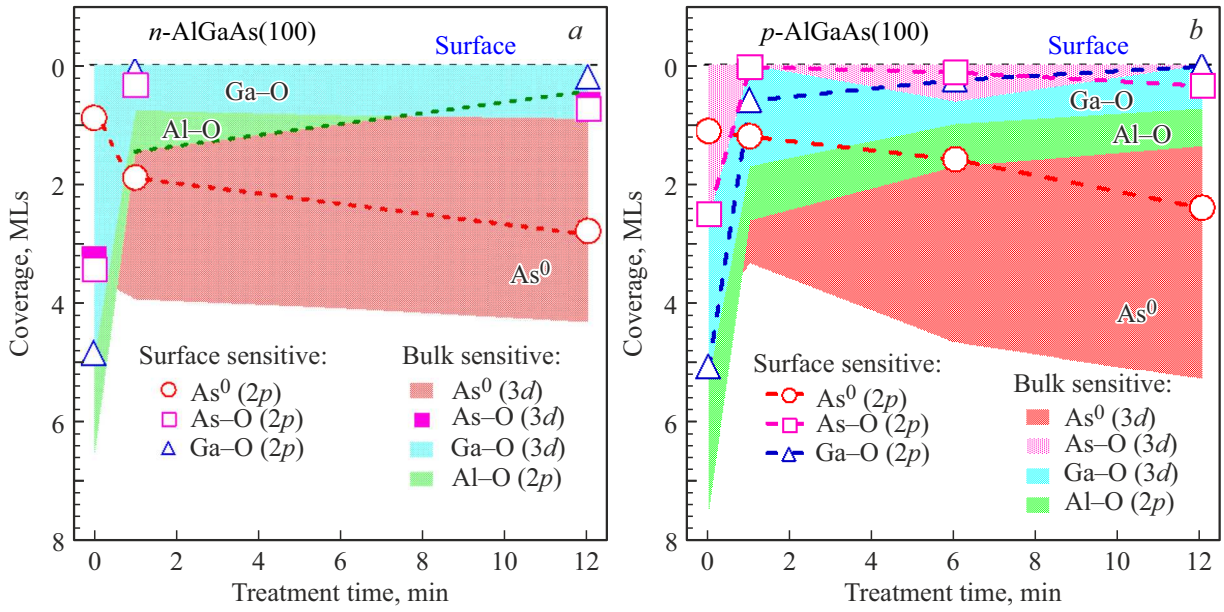

Figure 6. Changes in the thicknesses of various oxide layer components on the *n*- (*a*) and *p*-$Al_{0.3}Ga_{0.7}As(100)$ (*b*) surface after treatment with 4.7 M aqueous Na_2S, solution, calculated on the basis of decomposition of the bulk-sensitive As 3*d*, Ga 3*d* and Al 2*p* core level spectra [20], as well as the surface-sensitive As $2p_{3/2}$ and Ga $2p_{3/2}$ core level spectra.

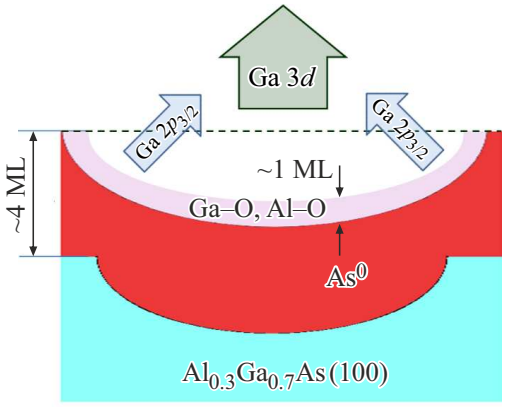

Figure 7. The scheme of photoelectron emission of the Ga $3d$ and Ga $2p_{3/2}$ core levels from a rough AlGaAs(100) surface.

observed increase in surface roughness (Figure 4), taking into account that the surface treatment with 4.7 M Na_2S aqueous solution does not lead to a significant change in the thickness of the elemental arsenic layer (Figure 6).

The rough surface is characterised by the presence of a large number of hollows and hills with height differences reaching several nanometres, comparable to the thickness of the elementary arsenic layer and the depth of the analyzed region for the photoelectrons of the Ga $2p_{3/2}$ ($3\lambda_{Ga2p} \approx 3.3$ nm) core level. The depth of the analyzed region for the Ga $3d$ compose $3\lambda_{Ga3d} \approx 9.1$ nm, i. e., noticeably higher than the observed values of height differences. Therefore, when analysing the Ga $3d$ core level spectra, the surface can be considered flat, while when analysing the Ga $2p_{3/2}$ core level spectra, it is necessary to take into account the roughness leading to an increase in the effective surface area (Figure 7). An increase in the effective surface area, however, will lead to a proportional decrease in the effective thickness of the gallium oxide layer, which was observed experimentally (Figure 6).

Sodium sulfide is a salt formed by a strong base (NaOH) and a weak acid (H_2S), so its aqueous solution has a strongly alkaline environment (pH $\geq$ 13), and the hydroxide ions OH^- available in such a solution in large quantities interact with gallium, aluminum and arsenic oxides, forming soluble hydroxide complexes [20] with them. This results in the removal of oxides without significantly changing the amount of elemental arsenic on the surface (Figure 6). The small As−O component (Figures 5, 6) observed in the spectra of the As $2p_{3/2}$ core level after treatment with sodium sulfide solution is most likely due to the undissolved arsenic hydroxide $As(OH)_3$ [27] formed after interaction with hydroxide ions in the sulfide solution. The gallium and aluminum oxide components remaining in the spectra of the surfaces after treatment with sodium sulfide solution may also contain contributions from the corresponding hydroxide [27,28].

Removal of the native oxide layer from the n-AlGaAs(100) surface occurs after contact with the solution for 1 min (Figure 6, a). Further soaking in the solution does not change the chemical composition of the surface layer (Figure 6, a), but leads to a significant increase in surface roughness (Figure 4) due to the rearrangement of the amorphous layer of elemental arsenic due to interaction with the solution. On the other hand, the removal of oxides from the p-AlGaAs(100) surface is slower (Figure 6, b) and the surface roughness of p-AlGaAs(100) changes in a more complex way (Figure 4). The fact that the rates of the native oxide layer removal from n- and p-type surfaces are different indicates a redox mechanism of oxide layer interaction with the aqueous sodium sulfide solution.

4. Conclusion

The morphology and composition of the oxide layer formed on $Al_{0.3}Ga_{0.7}As(100)$ surface under air exposure for several months as well as its evolution under treatment with concentrated aqueous sodium sulfide solution are investigated by atomic-force microscopy and X-ray photoelectron spectroscopy. It is shown that aluminum, gallium and arsenic oxides are located in the upper part of the native oxide layer, while the interface region of the oxide layer with the semiconductor surface consists mainly of elemental arsenic. Treatment with 4.7 M aqueous sodium sulfide solution causes almost complete removal of oxides and does not significantly change the thickness of the arsenic layer. The surface remains covered with the elemental arsenic coat $\sim$ 1 nm thick, the roughness of which increases as the processing time increases.

Acknowledgments

Equipment provided by the „Physical Methods of Surface Investigation“ resource center (St. Petersburg State University) was used in the study.

Conflict of interest

The authors declare that they have no conflict of interest.

References

[1] R.W. Lambert, T. Ayling, A.F. Hendry, J.M. Carson, D.A. Barrow, S. McHendry, C.J. Scott, A. McKee, W. Meredith. J. Lightwave Technol., **24**, 61 (2006).
[2] S. Koseki, B. Zhang, K. De Greve, Y. Yamamoto. Appl. Phys. Lett., **94**, 051110 (2009).
[3] I.E. Cortes-Mestizo, L.I. Espinosa-Vega, J.A. Espinoza-Figueroa, A. Cisneros-de-la-Rosa, E. Eugenio-Lopez, V.H. Mendez-Garcia, E. Briones, J. Briones, L. Zamora-Peredo, R. Droopad, C. Yee-Rendon. J. Vac. Sci. Technol., B, **34**, 02L110 (2016).
[4] G. Mariani, P.-S. Wong, A.M. Katzenmeyer, F. Léonard, J. Shapiro, D.L. Huffaker. Nano Lett., **11**, 2490 (2011).
[5] L. Shen, E.Y.B. Pun, J.C. Ho. Mater. Chem. Front., **1**, 630 (2017).
[6] E. Barrigón, M. Heurlin, Z. Bi, B. Monemar, L. Samuelson. Chem. Rev., **119**, 9170 (2019).

[7] G. Boras, X. Yu, H.A. Fonseka, G. Davis, A.V. Velichko, J.A. Gott, H. Zeng, S. Wu, P. Parkinson, X. Xu, D. Mowbray, A.M. Sanchez, H. Liu. J. Phys. Chem. C, **125**, 14338 (2021).
[8] R.R. Reznik, I.V. Ilkiv, K.P. Kotlyar, V.O. Gridchin, D.N. Bondarenko, V.V. Lendyashova, E.V. Ubyivovk, A.S. Dragunova, N.V. Kryzhanovskaya, G.E. Cirlin. Phys. Status Solidi RRL, **16**, 2200056 (2022).
[9] A. Creti, P. Prete, N. Lovergine, M. Lomascolo. ACS Appl. Nano Mater., **5**, 18149 (2022).
[10] K. Minehisa, R. Murakami, H. Hashimoto, K. Nakama, K. Sakaguchi, R. Tsutsumi, T. Tanigawa, M. Yukimune, K. Nagashima, T. Yanagida, S. Sato, S. Hiura, A. Murayama, F. Ishikawa. Nanoscale Adv., **5**, 1651 (2023).
[11] Y. Sun, P. Pianetta, P.-T. Chen, M. Kobayashi, Y. Nishi, N. Goel, M. Garner, W. Tsai. Appl. Phys. Lett., **93**, 194103 (2008).
[12] A. Nainani, Y. Sun, T. Irisawa, Z. Yuan, M. Kobayashi, P. Pianetta, B.R. Bennet, J.B. Boos, K.C. Saraswat. J. Appl. Phys., **109**, 114908 (2011).
[13] F.S. Aguirre-Tostado, M. Milojevic, C.L. Hinkle, E.M. Vogel, R.M. Wallace, S. McDonnel, C.J. Hughes. Appl. Phys. Lett., **92**, 171906 (2008).
[14] M.V. Lebedev, N.A. Kalyuzhnyy, S.A. Mintairov, W. Calwet, B. Kaiser, W. Jaegermann. Mater. Sci. Semicond. Process., **51**, 81 (2016).
[15] V.L. Berkovits, V.M. Lantratov, T.V. L'vova, G.A. Shakiashvili, V.P. Ulin, D. Paget. Appl. Phys. Lett., **63**, 970 (1993).
[16] I.V. Sedova, T.V. L'vova, V.P. Ulin, S.V. Sorokin, A.V. Ankudinov, V.L. Berkovits, S.V. Ivanov, P.S. Kop'ev. Semiconductors, **36**, 54 (2002).
[17] T.V. L'vova, I.V. Sedova, M.S. Dunaevskii, A.N. Karpenko, V.P. Ulin, S.V. Ivanov, V.L. Berkovits. Phys. Solid State, **51**, 1114 (2009).
[18] V.A. Solov'ev, I.V. Sedova, T.V. Lvova, M.V. Lebedev, P.A. Dement'ev, A.A. Sitnikova, A.N. Semenov, S.V. Ivanov. Appl. Surf. Sci., **356**, 378 (2015).
[19] H. Oigawa, J.-F. Fan, Y. Nannichi, H. Sugahara, M. Oshima. Jpn. J. Appl. Phys., **30**, L322 (1991).
[20] M.V. Lebedev, T.V. Lvova, I.V. Sedova, Yu.M. Serov, S.V. Sorokin, A.V. Koroleva, E.V. Zhizhin, S.V. Lebedev. Mater. Sci. Semicond. Process., **181**, 108604 (2024).
[21] C.J. Powell, A. Jablonski. Nucl. Instrum. Meth. Phys. Res. A, **601**, 54 (2009).
[22] C.J. Powell, A. Jablonski. *NIST Electron Inelastic-Mean-Free-Path Database* — Version 1.2 [National Institute of Standards and Technology, Gaithersburg, MD (2010)].
[23] M.V. Lebedev. Semiconductors **54**, 699 (2020).
[24] C.D. Thurmond, G.P. Schwartz, G.W. Kammlott, B. Schwartz. J. Electrochem. Soc., **127**, 1366 (1980).
[25] R. Toyoshima, S. Murakami, S. Eguchi, K. Amemiya, K. Mase, H. Kondoh. Chem. Commun., **56**, 14905 (2020).
[26] M. Scarrozza, G. Pourtois, M. Houssa, M. Caymax, A. Stesmans, M. Meuris, M.M. Heyns. Appl. Phys. Lett., **95**, 253504 (2009).
[27] M.V. Lebedev, E. Mankel, T. Mayer, W. Jaegermann. J. Phys. Chem. C, **114**, 21385 (2010).
[28] P.M.A. Sherwood. Surf. Sci. Spectra, **5**, 1 (1998).

Translated by J.Savelyeva